GEOLOGY | THE GEOLOGICAL SOCIETY OF AMERICA®

https://doi.org/10.1130/G49860.1

Manuscript received 3 November 2021
Revised manuscript received 13 January 2022
Manuscript accepted 26 February 2022

Published online 6 May 2022

Nd isotopic evidence for enhanced mafic weathering leading to Ordovician cooling

Christopher T. Conwell[1]*, Matthew R. Saltzman[1], Cole T. Edwards[2], Elizabeth M. Griffith[1] and Y. Datu Adiatma[1]
[1]School of Earth Sciences, The Ohio State University, Mendenhall Laboratory, 125 South Oval Mall, Columbus, Ohio 43210, USA
[2]Department of Geological and Environmental Sciences, Appalachian State University, 033 Rankin Science West, ASU Box 32067, Boone, North Carolina 28608, USA

ABSTRACT

It remains unclear whether waning of the volcanic degassing CO_2 source or enhancement of the mafic (Ca, Mg-silicate) weathering CO_2 sink, or both, caused global cooling leading to the Ordovician greenhouse–icehouse transition. We present a uniquely age-constrained and integrated Middle–Late Ordovician (470–450 Ma) continental weathering isotopic proxy data set ($^{87}Sr/^{86}Sr$ and $\varepsilon_{Nd(t)}$) from carbonate rocks of the Antelope Range of central Nevada, USA, paired with published paleotemperature proxy measurements ($\delta^{18}O$) of conodont apatite from the same locality. This suite of proxy records signals an increase in mafic weathering of the Taconic mountains (eastern United States) at ca. 463 Ma, which forced a period of global cooling. We adapt a $^{87}Sr/^{86}Sr$ and pCO_2 mass balance approach to model CO_2 drawdown during the Ordovician, and show that a combined decrease in volcanic degassing and increase in mafic weathering approximately halves pCO_2 in agreement with $\delta^{18}O$ trends and paleotemperature reconstructions.

INTRODUCTION

Carbon cycle models (Goddéris and Donnadieu, 2019; Isson et al., 2020) and geochemical, tectonic, and paleogeographic data sets (Kent and Muttoni, 2008; Cox et al., 2016; Jagoutz et al., 2016; Swanson-Hysell and Macdonald, 2017; Macdonald et al., 2019; Park et al., 2020) suggest that changes in global weatherability through the exposure of mafic (Ca, Mg-silicate) rocks at low latitude may be a primary driver of changes in Earth's long-term climate state. However, analyses of detrital zircon age distributions (McKenzie et al., 2016), refinement of continental volcanic arc activity and inferred degassing fluxes through time (Lee and Lackey, 2015; Pohl et al., 2020), and models of reverse weathering (Isson et al., 2020) have been interpreted to support the hypothesis that CO_2 sources, rather than sinks, represent the primary drivers of long-term climate.

This controversy presents itself in studying the cause of the Ordovician greenhouse–icehouse transition, a ~15 °C (~+3.5‰ $\delta^{18}O$) global cooling event (Grossman and Joachimski, 2020; Edwards et al., 2021; Goldberg et al., 2021; Männik et al., 2021; Fig. 1) that has been independently explained both by enhanced silicate weathering (Young et al., 2009; Nardin et al., 2011; Swanson-Hysell and Macdonald, 2017; Goddéris and Donnadieu, 2019) and decreased volcanic degassing (McKenzie et al., 2016). The Middle–Late Ordovician Taconic orogeny (ca. 470–450 Ma) has been cited as a probable cause of enhanced terrestrial silicate weathering, featuring uplift of ophiolites on the Taconic (southern Laurentian) margin that would have increased the presence of weatherable mafic rocks at low latitude, where weathering rates are highest (Young et al., 2009; Swanson-Hysell and Macdonald, 2017; Macdonald et al., 2019; Figs. 1A and 1B). The timing of a shift in weathering provenance attributed to Taconic uplift has been constrained by extensive measurements of proxy signals including seawater $^{87}Sr/^{86}Sr$ (Young et al., 2009; Saltzman et al., 2014), detrital (shale) $^{143}Nd/^{144}Nd$ [as $\varepsilon_{Nd(t)}$] (Patchett et al., 1999; Swanson-Hysell and Macdonald, 2017), detrital chromite (Hiscott, 1984), and whole-rock shale geochemistry (Garver et al., 1996). However, detrital $\varepsilon_{Nd(t)}$ records weathering source provenance within a graptolite-based age framework (or with ages directly tied to radiometrically dated horizons; Swanson-Hysell and Macdonald, 2017), whereas carbonate records preserve seawater or early diagenetic porewater chemistry within a conodont-based framework that allows for direct comparison to seawater proxy signals like $^{87}Sr/^{86}Sr$ and $\delta^{18}O$ in the same samples. Separate age frameworks may introduce considerable temporal uncertainty that hinders a multi-proxy approach to the study of Ordovician weathering and climate patterns. Furthermore, paleotemperature proxy data are sparse throughout this interval of changing weathering source lithology (Swanson-Hysell and Macdonald, 2017; Grossman and Joachimski, 2020), and more data are needed to constrain the timing of Ordovician cooling to test hypotheses of drivers of global climate during the Middle–Late Ordovician.

In our study, we integrated records of silicate weathering and paleotemperature across an interval of Middle–Late Ordovician cooling by pairing new high-resolution bulk carbonate $^{87}Sr/^{86}Sr$ and $\varepsilon_{Nd(t)}$ measurements with published $\delta^{18}O$ measurements of conodont apatite from a single stratigraphic section in the Antelope Range of central Nevada (USA). We used an integrated Ordovician isotope proxy data set as a unique case study to test the hypothesis that Earth's long-term climate system responds to changes in the predominance of mafic weathering, as suggested by conceptual and numerical models (e.g., Isson et al., 2020).

BACKGROUND AND METHODS

Seawater $^{87}Sr/^{86}Sr$ and $\varepsilon_{Nd(t)}$ are primarily controlled by the isotopic composition of crustal lithologies exposed on the continents, the dissolved weathering products of which are delivered to the ocean by continental runoff (Goldstein and Jacobsen, 1987). $^{87}Sr/^{86}Sr$ is secondarily influenced by a mid-ocean ridge hydrothermal flux. Therefore, pairing this signal

*E-mail: conwell.30@osu.edu

CITATION: Conwell, C.T., et al., 2022, Nd isotopic evidence for enhanced mafic weathering leading to Ordovician cooling: Geology, v. 50, p. 886–890, https://doi.org/10.1130/G49860.1

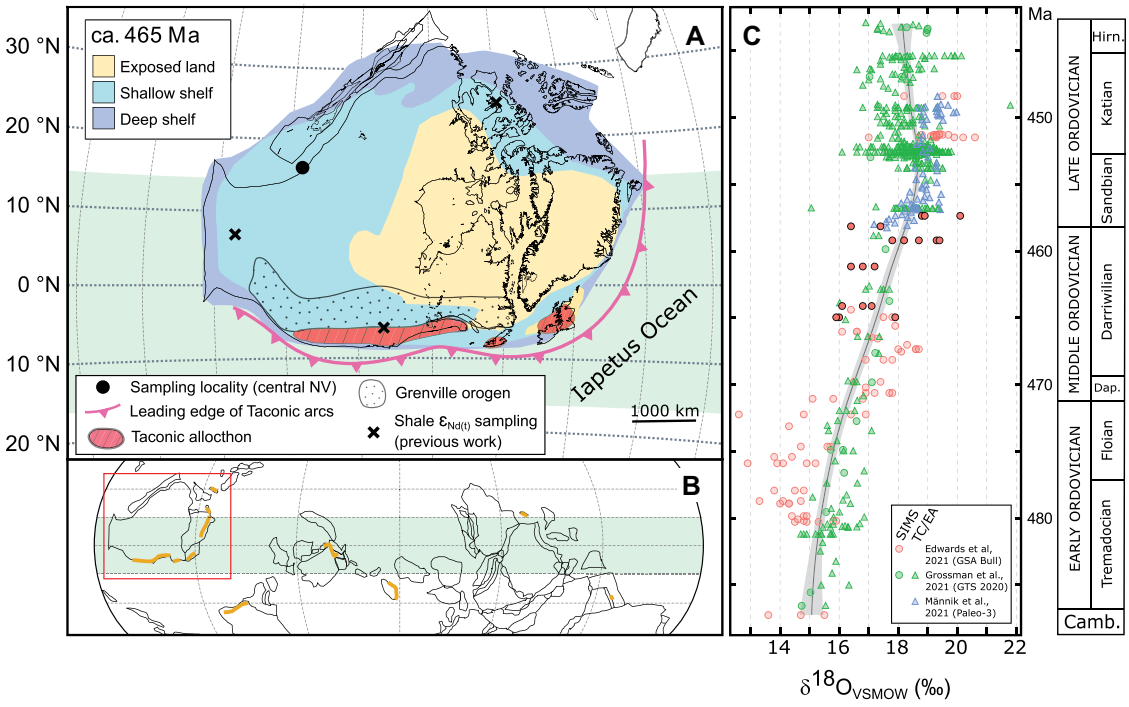

Figure 1. (A) Map of Laurentia at ca. 465 Ma (modified from Swanson-Hysell and Macdonald, 2017) showing the extent of the Taconic accretionary margin (red), throughout which ophiolites and mafic/ultramafic rocks occur. The leading edge of accreting terranes (pink line with teeth on overriding lithosphere) shows the approximate position of the Taconic island arc system (Swanson-Hysell and Macdonald, 2017). Shelf depth zonation is adapted from Torsvik and Cocks (2016), and the Grenville orogen extent is adapted from Gehrels and Pecha (2014). Green band represents humid tropical latitudes following Macdonald et al. (2019). Selected shale $\varepsilon_{Nd(t)}$ sampling localities are from a data compilation by Swanson-Hysell and Macdonald (2017). (B) Global map of continental crustal bodies at 465 Ma modified from Macdonald et al. (2019). Orange lines mark stretches of continental margin bearing ophiolites (Macdonald et al., 2019). Laurentia is boxed in red. (C) Compiled $\delta^{18}O$ measurements of Ordovician conodont apatite. Corrections applied to secondary ion mass spectrometer (SIMS) measurements are -1‰ (Edwards et al., 2021) and -0.6‰ (Grossman and Joachimski, 2020) to allow proper comparison to temperature conversion elemental analyzer (TC/EA) isotope ratio mass spectrometry measurements. A locally weighted scatterplot smoothing (LOESS) curve (black line) is plotted with a 95% confidence interval (gray band) using the "loess" function of the R package "stats" (3.6.2, https://www.rdocumentation.org/packages/stats/versions/3.6.2). Pink filled circles are from the Antelope Range section in Nevada, USA (Edwards et al., 2021) and are shown in Figure 2C.

with $\varepsilon_{Nd(t)}$, which has a negligible hydrothermal flux (Goldstein and Jacobsen, 1987), helps to interpret the record of continental weathering. Sr is largely homogenous in the global ocean (Allègre et al., 2010), whereas Nd varies between water masses due to its shorter residence time and provides information on regional changes in weathering source lithology (Goldstein and Jacobsen, 1987).

See the Supplemental Material[1] for an expanded description of the methods and background, which are briefly summarized here. We sampled a ~220-m-thick and relatively continuous succession of Middle–Late Ordovician passive margin, deep-subtidal carbonate strata in the Antelope Range of central Nevada (Young et al., 2009; Saltzman et al., 2014; Fig. 1A). Bulk carbonate $^{87}Sr/^{86}Sr$ and $\varepsilon_{Nd(t)}$ were measured with a ThermoFisher Triton Plus thermal ionization mass spectrometer at The Ohio State University (Ohio, USA). Published $^{87}Sr/^{86}Sr$ and $\delta^{18}O$ measurements from this section align well with compiled data sets, suggesting that proxy records in bulk rock and conodonts at this locality record primary signals.

RESULTS

$^{87}Sr/^{86}Sr$ values from the Antelope Range section of central Nevada were measured in bulk carbonate spanning 471–465 Ma (Fig. 2A). Measurements younger than 465 Ma are from Saltzman et al. (2014), who reported $^{87}Sr/^{86}Sr$ in conodont apatite from this section. $^{87}Sr/^{86}Sr$ decreases steadily from 0.70872 at 465 Ma to 0.70797 at 453 Ma, marking one of the most prominent periods of seawater $^{87}Sr/^{86}Sr$ change in the Phanerozoic. $\varepsilon_{Nd(t)}$ measurements of the acid-soluble portion of bulk carbonate samples spanning 470–463 Ma demonstrate a steady pre-shift baseline at $\varepsilon_{Nd(t)} = -18.5 \pm 0.5$ (Fig. 2B). At 463 Ma, values rise sharply from baseline to $\varepsilon_{Nd(t)} = \sim -12 \pm 4$ at ca. 455.5 Ma, similar to post-shift shale $\varepsilon_{Nd(t)}$ values across Laurentia (Patchett et al., 1999; Swanson-Hysell and Macdonald, 2017).

DISCUSSION

Isotope Proxy Evidence for Enhanced Mafic Weathering

The shift in globally influenced seawater $^{87}Sr/^{86}Sr$ to lower (less radiogenic) values, and regionally influenced $\varepsilon_{Nd(t)}$ to higher (more radiogenic) values, at 463 Ma suggests that both signals are linked to a mafic weathering driver. Such a shift could have resulted from low-latitude, arc-continent collision during the Taconic orogeny, which initiated at ca. 465 Ma (Young et al., 2009; Swanson-Hysell and Macdonald, 2017). Our bulk carbonate $^{87}Sr/^{86}Sr$ and $\varepsilon_{Nd(t)}$ measurements align well with Laurentian compilations (Saltzman et al., 2014; Edwards et al., 2015; Swanson-Hysell and Macdonald, 2017), supporting the preservation of primary signals. It is possible that the acid-soluble portion of our samples includes Nd leached from residual terrigenous material and that the shift in our carbonate $\varepsilon_{Nd(t)}$ record may reflect the arrival of Taconic detritus with a shift to more argillaceous carbonates in the Copenhagen Formation rather than the evolution of seawater $\varepsilon_{Nd(t)}$ (Abbott et al., 2022; see the Supplemental Material). However, this still demonstrates a shift to a more mafic weathering source lithology and allows for direct comparison to $^{87}Sr/^{86}Sr$ and $\delta^{18}O$ seawater signals within a unified age framework. Regional carbonate $\varepsilon_{Nd(t)}$ could have also been affected by weathering of Neoproterozoic Grenville crust ($\varepsilon_{Nd(t)} = \sim -6$; Patchett et al., 1999) comprising the Laurentian margin or by mixing with Iapetus waters having a distinct $\varepsilon_{Nd(t)}$ composition. However, bulk rock geochemical evidence suggests a primary influence from uplifted mafic rocks (Hiscott, 1984; Garver et al., 1996), and the

[1]Supplemental Material. Extended methods and discussion, supplemental figures, and tables of isotope data and model parameters and outputs. Please visit https://doi.org/10.1130/GEOL.S.19579441 to access the supplemental material, and contact editing@geosociety.org with any questions.

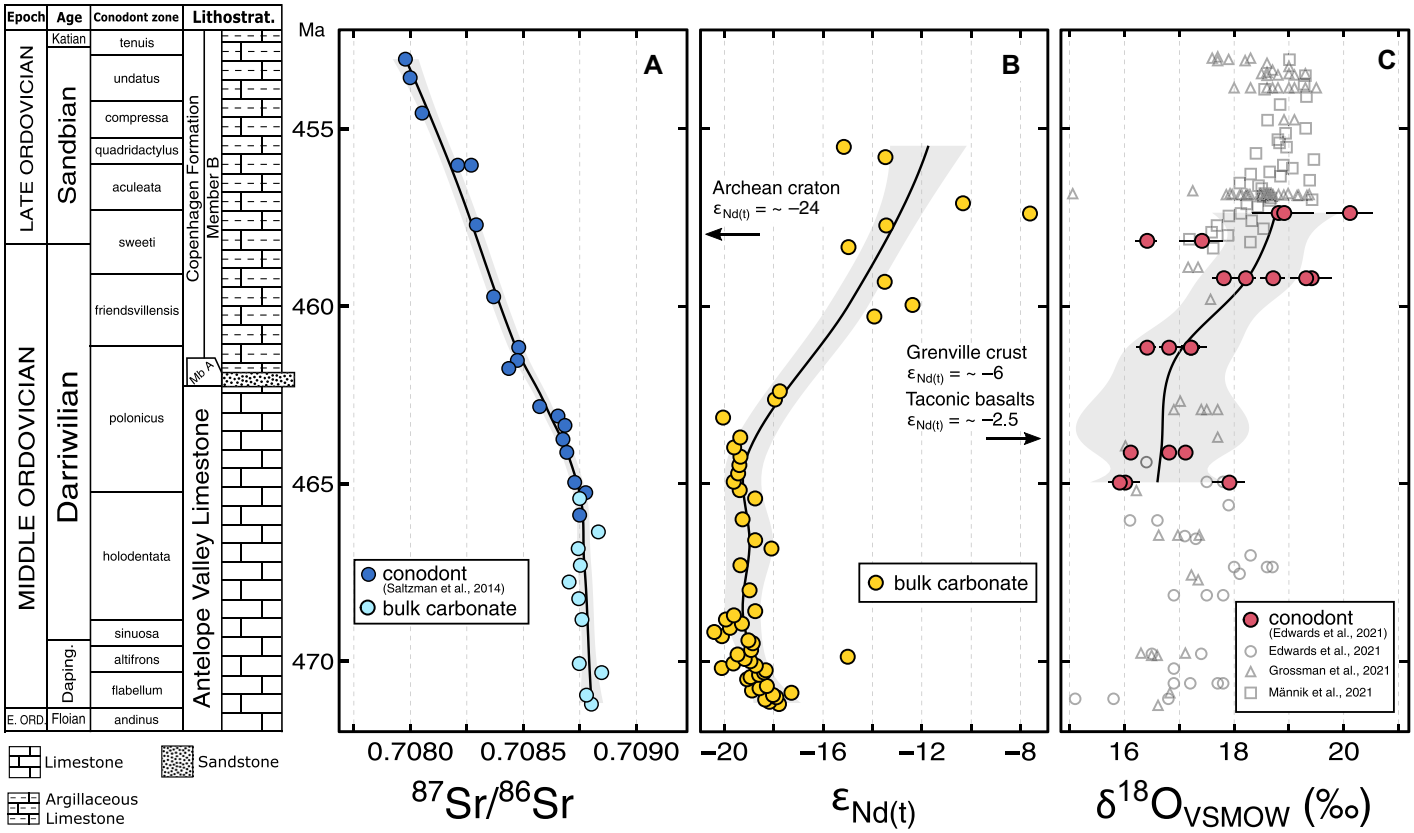

Figure 2. Paired $^{87}Sr/^{86}Sr$, $\varepsilon_{Nd(t)}$, and $\delta^{18}O$ measurements from the Antelope Range of central Nevada (USA). Trendlines are locally weighted scatterplot smoothing (LOESS) curves (black line) with a 95% confidence interval (gray band). (A) $^{87}Sr/^{86}Sr$ measured in the acid-soluble portions of bulk carbonate rock and conodont apatite. Conodont measurements are from Saltzman et al. (2014). (B) $\varepsilon_{Nd(t)}$ measurements of the acid-soluble portion of bulk carbonate rock. Arrows point to $\varepsilon_{Nd(t)}$ of Laurentian crustal provinces (Patchett et al., 1999). (C) $\delta^{18}O$ measurements of conodont apatite from Edwards et al. (2021). Red dots are an average of several ($n \geq 7$) spot analyses of a single conodont element, with error bars showing the standard error of the mean. Open gray symbols are from the compilation shown in Figure 1C. The LOESS curve is based on the red dots only.

$^{87}Sr/^{86}Sr$ signature of Grenville crust (>0.710) is too radiogenic to create the observed trend in seawater $^{87}Sr/^{86}Sr$ (see the Supplemental Material). Additionally, the agreement of the shift in our carbonate $\varepsilon_{Nd(t)}$ record with previously observed shifts in detrital (shale) $\varepsilon_{Nd(t)}$ records of Laurentian basins opposes the possibility of a water mass mixing driver of regional carbonate $\varepsilon_{Nd(t)}$ (e.g., Fanton et al., 2002), further supporting a Taconic driver. The dominance of global seawater $^{87}Sr/^{86}Sr$ by a regional event such as weathering of mafic crust in the Taconic orogen is consistent with the outsized role of mafic weathering in regulating seawater $^{87}Sr/^{86}Sr$ (Allègre et al., 2010) as well as previous efforts to model Ordovician seawater $^{87}Sr/^{86}Sr$ (Young et al., 2009; Nardin et al., 2011).

The ~2.7‰ increase in the Antelope Range $\delta^{18}O$ record corresponds to an ~11 °C cooling (Pucéat et al., 2010), which is dramatic in comparison to the ~3.5‰ increase throughout the whole Ordovician shown in recent $\delta^{18}O$ compilations (Fig. 1C). The influence of glaciation on our $\delta^{18}O$ record is difficult to constrain, and the timing of the onset of Ordovician glaciation is still an active question. However, recent studies of Ordovician paleoclimate records suggest that glaciation may have begun as early as the late Middle Ordovician (Darriwilian stage) (Dabard et al., 2015; Rasmussen et al., 2016; Pohl et al., 2016), which matches the timing of shifts in our weathering proxy records and deposition of the basal sandstone of the Copenhagen Formation and possibly marks a sea-level lowstand (Fig. 2; see the Supplemental Material). Clumped isotope records reveal a shift in Late Ordovician seawater $\delta^{18}O$ by as much as +3–4‰, but data through the Middle Ordovician are scarce (Finnegan et al., 2011; Bergmann et al., 2018). A sea-level lowstand caused by Darriwilian ice-sheet growth would further expose the Taconic margin to weathering, thus constituting a positive feedback leading to enhanced mafic weathering and CO_2 drawdown. If true, the observed shift in the $\delta^{18}O$ record would reflect, at least in part, the pronounced growth of Ordovician ice sheets. The apparent ~2 m.y. lag of a shift in the $\delta^{18}O$ record following the shift in weathering proxy signals may be an artifact of data scarcity or may accurately reflect dynamics of carbon sources, sinks, and feedbacks (see the Supplemental Material).

Implications for Middle–Late Ordovician Carbon Cycling

We adapted the weatherability-driven seawater $^{87}Sr/^{86}Sr$ and atmospheric pCO_2 mass balance model of Young et al. (2009) to test hypotheses of Ordovician silicate weathering and volcanic degassing (Fig. 3; weatherability is defined as the sum of factors that influence silicate weathering rate, except climate). We use the original model framework, which features a slow decline in $^{87}Sr/^{86}Sr$ of the riverine flux in the Early–Middle Ordovician attributed to non-Laurentian weathering sources (Young et al., 2009). The Young et al. (2009) model then introduces a Taconic perturbation that increases a weatherability parameter by 25% (constrained by Sr isotope mass balance; Fig. 3B; Fig. S1 in the Supplemental Material), increasing the contribution of mafic weathering ($^{87}Sr/^{86}Sr = 0.7043$) and shifting the riverine Sr flux to lower values from its pre-shift $^{87}Sr/^{86}Sr$ value of 0.7106. In addition to the shift to mafic weathering proxy signatures, a 25% increase in global weatherability is further supported by paleogeographic data sets indicating that continental area (Nardin et al., 2011; Goddéris and Donnadieu, 2019;

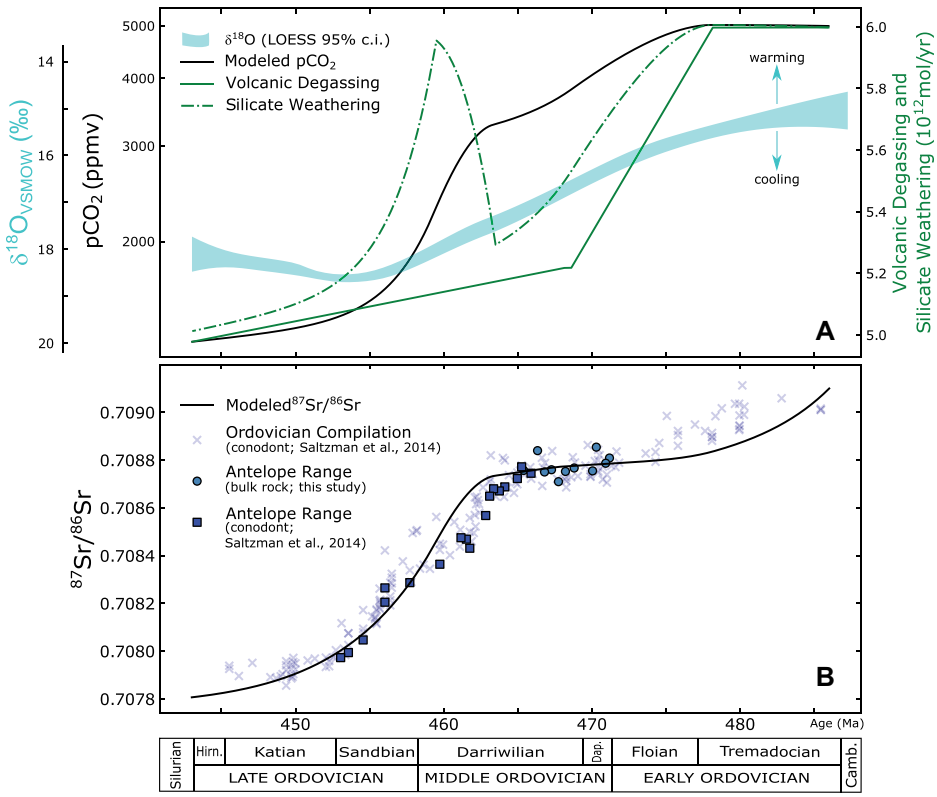

Figure 3. (A) Model scenario of volcanic degassing source and silicate weathering sink fluxes and the resulting evolution of atmospheric pCO_2. Volcanic degassing is a tuneable parameter based on arc-related zircon reconstructions (Marcilly et al., 2021), whereas silicate weathering varies as a function of weatherability and pCO_2 (Young et al., 2009). Blue band is the 95% confidence interval of the smoothing curve applied to $\delta^{18}O$ measurements plotted in Figure 1C. Note the logarithmic scaling of the pCO_2 *y*-axis. (B) $^{87}Sr/^{86}Sr$ model output and data. $^{87}Sr/^{86}Sr$ model output (black line) is achieved using the equations of Young et al. (2009) with volcanic degassing and silicate weathering fluxes shown in panel A (see also Fig. S1 and Table S2 [see footnote 1]). Blue squares are $^{87}Sr/^{86}Sr$ measurements of conodont apatite from Saltzman et al. (2014), which includes the measurements of conodont apatite in Figure 2A.

Marcilly et al., 2021) and ophiolite exposure (Swanson-Hysell and Macdonald, 2017; Macdonald et al., 2019) at low latitude reached a Phanerozoic high at ca. 460 Ma. To test the model against updated records of volcanic degassing and paleotemperature, we used a new degassing scenario based on arc-derived zircon age populations (Marcilly et al., 2021) (Fig. S2) and compare the pCO_2 results of our model to compiled $\delta^{18}O$ measurements (Fig. 1C). Atmospheric pCO_2 decreases from 18 to 4.7 times present atmospheric level (PAL; 1 PAL = 280 ppmv CO_2) throughout the model run, which is similar to existing Phanerozoic pCO_2 models (Goddéris and Donnadieu, 2019). Although our model presents a non-unique solution, the agreement of trends in $^{87}Sr/^{86}Sr$ and pCO_2 model results with observed $^{87}Sr/^{86}Sr$ and $\delta^{18}O$ measurements supports the plausibility of a mafic weathering driver of Middle–Late Ordovician cooling (Fig. 3B). Our model does not capture the influence of paleogeography, which may also explain the Early Ordovician $\delta^{18}O$ cooling trend as observed in spatially resolved model frameworks (Nardin et al., 2011; Goddéris and Donnadieu, 2019). Neither does our pCO_2 model account for CO_2 sources such as reverse weathering or sulfide oxidation, nor does it parametrize certain CO_2 sinks such as the rise of non-vascular land plants (Isson et al., 2020). For further discussion of model parameters, results, sensitivity, and conversion of $\delta^{18}O$ to paleotemperature, see the Supplemental Material.

CONCLUSIONS

Pairing silicate weathering and paleotemperature proxy signals in marine precipitates from a single stratigraphic section gives new insight into the link between mafic weathering and long-term climate. Large shifts in the seawater $^{87}Sr/^{86}Sr$ and $\varepsilon_{Nd(t)}$ composition of the Laurentian Sea during the Middle–Late Ordovician clearly demonstrate a change in weathering source lithology during a time of extensive uplift of mafic oceanic crust at tropical latitudes. Previous conodont $\delta^{18}O$ measurements from this same section (Edwards et al., 2021) allow unique observation of the coupling of weathering and paleotemperature proxies, indicating that weathering of uplifted mafic oceanic crust on the Taconic margin drove a pronounced cooling that led to the first major glaciation of the Phanerozoic. Furthermore, the posited role of declining degassing in Early–Middle Ordovician cooling highlights the importance of the integrated development of proxies for both CO_2 sources and sinks.

ACKNOWLEDGMENTS

Thoughtful comments from Alexandre Pohl, two anonymous reviewers, and editor Gerald Dickens greatly improved this paper. We thank Jeff Linder, Samantha Carter, and Teresa Avila for helpful discussions, and Anthony Lutton and John Olesik for help with inductively coupled–mass spectrometry analyses. Funding for thermal ionization mass spectrometry analyses and field sampling was provided by Friends of Orton Hall in the School of Earth Sciences at The Ohio State University.

REFERENCES CITED

Abbott, A.N., Löhr, S.C., Payne, A., Kumar, H., and Du, J., 2022, Widespread lithogenic control of marine authigenic neodymium isotope records? Implications for paleoceanographic reconstructions: Geochimica et Cosmochimica Acta, v. 319, p. 318–336, https://doi.org/10.1016/j.gca.2021.11.021.

Allègre, C.J., Louvat, P., Gaillardet, J., Meynadier, L., Rad, S., and Capmas, F., 2010, The fundamental role of island arc weathering in the oceanic Sr isotope budget: Earth and Planetary Science Letters, v. 292, p. 51–56, https://doi.org/10.1016/j.epsl.2010.01.019.

Bergmann, K.D., Finnegan, S., Creel, R., Eiler, J.M., Hughes, N.C., Popov, L.E., and Fischer, W.W., 2018, A paired apatite and calcite clumped isotope thermometry approach to estimating Cambro–Ordovician seawater temperatures and isotopic composition: Geochimica et Cosmochimica Acta, v. 224, p. 18–41, https://doi.org/10.1016/j.gca.2017.11.015.

Cox, G.M., Halverson, G.P., Stevenson, R.K., Vokaty, M., Poirier, A., Kunzmann, M., Li, Z.-X., Denyszyn, S.W., Strauss, J.V., and Macdonald, F.A., 2016, Continental flood basalt weathering as a trigger for Neoproterozoic Snowball Earth: Earth and Planetary Science Letters, v. 446, p. 89–99, https://doi.org/10.1016/j.epsl.2016.04.016.

Dabard, M.P., Loi, A., Paris, F., Ghienne, J.F., Pistis, M., and Vidal, M., 2015, Sea-level curve for the Middle to early Late Ordovician in the Armorican Massif (western France): Icehouse third-order glacio-eustatic cycles: Palaeogeography, Palaeoclimatology, Palaeoecology, v. 436, p. 96–111, https://doi.org/10.1016/j.palaeo.2015.06.038.

Edwards, C.T., Saltzman, M.R., Leslie, S.A., Bergström, S.M., Sedlacek, A.R.C., Howard, A., Bauer, J.A., Sweet, W.C., and Young, S.A., 2015, Strontium isotope ($^{87}Sr/^{86}Sr$) stratigraphy of Ordovician bulk carbonate: Implications for preservation of primary seawater values: Geological Society of America Bulletin, v. 127, p. 1275–1289, https://doi.org/10.1130/B31149.1.

Edwards, C.T., Jones, C.M., Quinton, P.C., and Fike, D.A., 2021, Oxygen isotope ($\delta^{18}O$) trends measured from Ordovician conodont apatite using secondary ion mass spectrometry (SIMS): Implications for paleo-thermometry studies: Geological Society of America Bulletin, v. 134, p. 261–274, https://doi.org/10.1130/B35891.1.

Fanton, K.C., Holmden, C., Nowlan, G.S., and Haidl, F.M., 2002, $^{143}Nd/^{144}Nd$ and Sm/Nd stratigraphy of Upper Ordovician epeiric sea carbonates: Geochimica et Cosmochimica Acta, v. 66, p. 241–255, https://doi.org/10.1016/S0016-7037(01)00773-6.

Finnegan, S., Bergmann, K., Eiler, J.M., Jones, D.S., Fike, D.A., Eisenman, I., Hughes, N.C., Tripati,

A.K., and Fischer, W.W., 2011, The magnitude and duration of Late Ordovician–Early Silurian glaciation: Science, v. 331, p. 903–906, https://doi.org/10.1126/science.1200803.

Garver, J.I., Royce, P.R., and Smick, T.A., 1996, Chromium and nickel in shale of the Taconic foreland; a case study for the provenance of fine-grained sediments with an ultramafic source: Journal of Sedimentary Research, v. 66, p. 100–106, https://doi.org/10.1306/D42682C5-2B26-11D7-8648000102C1865D.

Gehrels, G., and Pecha, M., 2014, Detrital zircon U-Pb geochronology and Hf isotope geochemistry of Paleozoic and Triassic passive margin strata of western North America: Geosphere, v. 10, p. 49–65, https://doi.org/10.1130/GES00889.1.

Goddéris, Y., and Donnadieu, Y., 2019, A sink- or a source-driven carbon cycle at the geological timescale? Relative importance of palaeogeography versus solid Earth degassing rate in the Phanerozoic climatic evolution: Geological Magazine, v. 156, p. 355–365, https://doi.org/10.1017/S0016756817001054.

Goldberg, S.L., Present, T.M., Finnegan, S., and Bergmann, K.D., 2021, A high-resolution record of early Paleozoic climate: Proceedings of the National Academy of Sciences of the United States of America, v. 118, e2013083118, https://doi.org/10.1073/pnas.2013083118.

Goldstein, S.J., and Jacobsen, S.B., 1987, The Nd and Sr isotopic systematics of river-water dissolved material: Implications for the sources of Nd and Sr in seawater: Chemical Geology, v. 66, p. 245–272.

Grossman, E.L., and Joachimski, M.M., 2020, Oxygen isotope stratigraphy, *in* Gradstein, F.M., et al., eds., Geologic Time Scale 2020: Amsterdam, Elsevier, p. 279–307, https://doi.org/10.1016/B978-0-12-824360-2.00010-3.

Hiscott, R.N., 1984, Ophiolitic source rocks for Taconic-age flysch: Trace-element evidence: Geological Society of America Bulletin, v. 95, p. 1261–1267, https://doi.org/10.1130/0016-7606(1984)95<1261:OSRFTF>2.0.CO;2.

Isson, T.T., Planavsky, N.J., Coogan, L.A., Stewart, E.M., Ague, J.J., Bolton, E.W., Zhang, S., McKenzie, N.R., and Kump, L.R., 2020, Evolution of the global carbon cycle and climate regulation on Earth: Global Biogeochemical Cycles, v. 34, e2018GB006061, https://doi.org/10.1029/2018GB006061.

Jagoutz, O., Macdonald, F.A., and Royden, L., 2016, Low-latitude arc-continent collision as a driver for global cooling: Proceedings of the National Academy of Sciences of the United States of America, v. 113, p. 4935–4940, https://doi.org/10.1073/pnas.1523667113.

Kent, D.V., and Muttoni, G., 2008, Equatorial convergence of India and early Cenozoic climate trends: Proceedings of the National Academy of Sciences of the United States of America, v. 105, p. 16,065–16,070, https://doi.org/10.1073/pnas.0805382105.

Lee, C.-T.A., and Lackey, J.S., 2015, Global continental arc flare-ups and their relation to long-term greenhouse conditions: Elements, v. 11, p. 125–130, https://doi.org/10.2113/gselements.11.2.125.

Macdonald, F.A., Swanson-Hysell, N.L., Park, Y., Lisiecki, L., and Jagoutz, O., 2019, Arc-continent collisions in the tropics set Earth's climate state: Science, v. 364, p. 181–184, https://doi.org/10.1126/science.aav5300.

Männik, P., Lehnert, O., Nõlvak, J., and Joachimski, M.M., 2021, Climate changes in the pre-Hirnantian Late Ordovician based on $\delta^{18}O_{phos}$ studies from Estonia: Palaeogeography, Palaeoclimatology, Palaeoecology, v. 569, 110347, https://doi.org/10.1016/j.palaeo.2021.110347.

Marcilly, C.M., Torsvik, T.H., Domeier, M., and Royer, D.L., 2021, New paleogeographic and degassing parameters for long-term carbon cycle models: Gondwana Research, v. 97, p. 176–203, https://doi.org/10.1016/j.gr.2021.05.016.

McKenzie, N.R., Horton, B.K., Loomis, S.E., Stockli, D.F., Planavsky, N.J., and Lee, C.-T.A., 2016, Continental arc volcanism as the principal driver of icehouse-greenhouse variability: Science, v. 352, p. 444–447, https://doi.org/10.1126/science.aad5787.

Nardin, E., Godderis, Y., Donnadieu, Y., Hir, G.L., Blakey, R.C., Puceat, E., and Aretz, M., 2011, Modeling the early Paleozoic long-term climatic trend: Geological Society of America Bulletin, v. 123, p. 1181–1192, https://doi.org/10.1130/B30364.1.

Park, Y., Maffre, P., Goddéris, Y., Macdonald, F.A., Anttila, E.S.C., and Swanson-Hysell, N.L., 2020, Emergence of the Southeast Asian islands as a driver for Neogene cooling: Proceedings of the National Academy of Sciences of the United States of America, v. 117, p. 25,319–25,326, https://doi.org/10.1073/pnas.2011033117.

Patchett, P.J., Ross, G.M., and Gleason, J.D., 1999, Continental drainage in North America during the Phanerozoic from Nd isotopes: Science, v. 283, p. 671–673, https://doi.org/10.1126/science.283.5402.671.

Pohl, A., Donnadieu, Y., Le Hir, G., Ladant, J., Dumas, C., Alvarez-Solas, J., and Vandenbroucke, T.R.A., 2016, Glacial onset predated Late Ordovician climate cooling: Paleoceanography, v. 31, p. 800–821, https://doi.org/10.1002/2016PA002928.

Pohl, A., et al., 2020, Carbonate platform production during the Cretaceous: Geological Society of America Bulletin, v. 132, p. 2606–2610, https://doi.org/10.1130/B35680.1.

Pucéat, E., Joachimski, M.M., Bouilloux, A., Monna, F., Bonin, A., Motreuil, S., Morinière, P., Hénard, S., Mourin, J., and Dera, G., 2010, Revised phosphate–water fractionation equation reassessing paleotemperatures derived from biogenic apatite: Earth and Planetary Science Letters, v. 298, p. 135–142, https://doi.org/10.1016/j.epsl.2010.07.034.

Rasmussen, C.M.Ø., et al., 2016, Onset of main Phanerozoic marine radiation sparked by emerging Mid Ordovician icehouse: Scientific Reports, v. 6, 18884, https://doi.org/10.1038/srep18884.

Saltzman, M.R., Edwards, C.T., Leslie, S.A., Dwyer, G.S., Bauer, J.A., Repetski, J.E., Harris, A.G., and Bergström, S.M., 2014, Calibration of a conodont apatite-based Ordovician $^{87}Sr/^{86}Sr$ curve to biostratigraphy and geochronology: Implications for stratigraphic resolution: Geological Society of America Bulletin, v. 126, p. 1551–1568, https://doi.org/10.1130/B31038.1.

Swanson-Hysell, N.L., and Macdonald, F.A., 2017, Tropical weathering of the Taconic orogeny as a driver for Ordovician cooling: Geology, v. 45, p. 719–722, https://doi.org/10.1130/G38985.1.

Torsvik, T.H., and Cocks, L.R.M., 2016, Earth History and Palaeogeography: Cambridge, UK, Cambridge University Press, 317 p., https://doi.org/10.1017/9781316225523.

Young, S.A., Saltzman, M.R., Foland, K.A., Linder, J.S., and Kump, L.R., 2009, A major drop in seawater $^{87}Sr/^{86}Sr$ during the Middle Ordovician (Darriwilian): Links to volcanism and climate?: Geology, v. 37, p. 951–954, https://doi.org/10.1130/G30152A.1.

Printed in USA